Revision 1

Slawsonite–celsian–hyalophane assemblage from a picrite sill (Prague Basin, Czech Republic)

ZUZANA TASÁRYOVÁ,[1, 2,*] JIŘÍ FRÝDA,[1] VOJTĚCH JANOUŠEK [1, 2] AND MARTIN RACEK [2]

[1] Czech Geological Survey, Klárov 3, Praha 1, 118 21, Czech Republic

[2] Faculty of Science, Charles University in Prague, Albertov 6, Praha 2, 128 43, Czech Republic

* Present address: Czech Geological Survey, Klárov 3, Praha 1, 118 21, Czech Republic.
E-mail: zuzana.tasaryova@geology.cz

ABSTRACT

The first European occurrence of slawsonite is reported from a picrite sill within Upper Ordovician strata of the Prague Basin near the village of Rovina, Czech Republic. The rare slawsonite forms an interstitial phase in association with abundant celsian and hyalophane, replacing the original calcic plagioclase (bytownite). A study of this curious natural slawsonite–celsian–hyalophane assemblage provides a valuable insight into feldspar stability and petrogenesis.

Whole-rock geochemical signatures of the picrite sill and underlying doleritic basalt intrusion show conspicuous enrichment in Sr and Ba superimposed on normal basaltic multielement patterns. These two elements were most likely introduced by intergranular fluids during diffusional seafloor metasomatism (rodingitization and serpentinization) of the picrite. Strontian and barian feldspars precipitated directly from $BaO–SrO–H_2O$ bearing fluid, which caused decomposition of plagioclase to vuagnatite, aqueous SiO_2 and Al_2O_3 at $T \leq 350$ °C. Subsequently, vuagnatite decomposed to

hydrogrossular and excess SiO_2 was consumed by serpentinization of olivine. At the expense of aqueous Al_2O_3, serpentine reacted to chlorite closing the picrite alteration at 320–160 °C. Pressure did not exceed 0.5 GPa. The *in situ* EDS analyses indicate that the chemical composition of the slawsonite is $Sl_{91}Cn_3An_3Ab_3$ (core) to $Sl_{82}Cn_3An_4Ab_9Or_2$ (rim), the celsians range from $Cn_{96.9}An_{0.3}Ab_{0.2}Or_2Sl_{0.6}$ to $Cn_{76.3}An_{4.7}Ab_3Or_{15.7}Sl_{0.3}$, and the hyalophanes vary from $Cn_{72.2}An_{1.4}Ab_{5.1}Or_{21.1}Sl_{0.2}$ to $Cn_{57.3}An_{0.8}Ab_{3.1}Or_{38.5}Sl_{0.3}$.

Keywords: slawsonite, celsian, hyalophane, strontium and barium feldspars, vuagnatite, hydrogrossular, rodingitization, serpentinization, Prague Basin

Running title: Slawsonite–celsian–hyalophane assemblage from a picrite sill

INTRODUCTION

Feldspar can be assigned as a barian once its chemical analysis contains more than 2 wt% of BaO (Deer et al. 1992). Celsian ($BaAl_2Si_2O_8$; Cn) is an end-member of an extensive solid solution with K-feldspar ($KAlSi_3O_8$), whereby the term hyalophane (Hy) is used for intermediate compositions (10–80 mol% of Cn: Deer et al. 2001 or 15–75 mol% of Cn: Essene et al. 2005), with the remainder being dominated by Or prevailing over Ab. Furthermore, hyalophanes with > 50 mol% Cn are referred to as barian, and those with < 25 mol% Cn as potassian. Natural celsians and hyalophanes usually have a monoclinic symmetry. However, even triclinic polymorphs of hyalophane (with less than Cn_{30}) were found in nature (Gay and Roy 1968). Celsian structure resembles monoclinic body-centered Si–Al unit cells of anorthite, in which an addition of relatively small Ca^{2+}

leads to distortion of framework and origin of triclinic symmetry. Nevertheless, celsians do not show strict regularity in alternation of Si and Al atoms like anorthite but rather significant Al and Si disorder (Griffen and Ribbe 1976). An acceptance of large radius ion Ba^{2+} into celsian framework keep the monoclinic symmetry and explain why hyalophanes with < Cn_{30}, e.g., with prevalence of Ca^{2+}, have triclinic symmetry. Experimental works confirmed the solid solution between celsian and albite ($NaAlSi_3O_8$) but with a miscibility gap (Viswanathan and Harneit 1989). These results were applied to the ternary system $BaAl_2Si_2O_8$–$NaAlSi_3O_8$–$KAlSi_3O_8$ (Lagache and Catel 1992; Viswanathan 1992). According to the most recent summary (Essene et al. 2005), 8 four-feldspar and 24 three-feldspar assemblages may be stable in the system $BaAl_2Si_2O_8$–$CaAl_2Si_2O_8$–$NaAlSi_3O_8$–$KAlSi_3O_8$.

While the occurrence of Ba-bearing feldspars is relatively common, natural slawsonite ($SrAl_2Si_2O_8$; Sl) is extremely rare. It is isostructural with paracelsian ($BaAl_2Si_2O_8$) (Griffen et al. 1977; Matsubara 1985). Paracelsian is a metastable phase of the slawsonite–paracelsian series and reacts to celsian at 550 °C; however, its stability at a lower *T* remains a possibility (Lin and Foster 1968). Phase transition from the low-*T* triclinic to the moderate-*T* monoclinic structure of natural slawsonite at ambient pressure has been observed at 320 °C (Tagai et al. 1995). Monoclinic slawsonite is stable up to 500 °C (McCauley 2000) or 600 °C (Bambauer and Nager 1981), when it transforms into another monoclinic polymorph, Sr-celsian (melting T = 1650 °C), although the reaction has not yet been reversed. The Sr-celsian is isostructural with celsian but has no natural counterpart (McCauley 2000). Partial replacement of Sr by Ca has been reported in slawsonite from metamorphosed limestones in Wallowa County, Oregon (Griffen et al.

1977; Matsubara 1985) and from slawsonite veinlets cutting pectolite veinlets in metamorphosed xenoliths (glaucophane to pumpellyite–actinolite schist of the Ino Fm.) in Rendai, Japan (Nakajima et al. 1978; Matsubara 1985). Barium substitution was detected in slawsonite veinlets from xenolith in an ultramafic rock exposed in weakly metamorphosed rocks of the Ino Fm. in Sarusaka, Japan (Matsubara 1985; Tagai et al. 1995). Xenolith consisted of diopside, chlorite and altered sphene but was devoid of igneous texture and was not considered as primary magmatic product (Matsubara 1985).

In this paper, we report the mode of occurrence and chemical composition of a rare assemblage of strontian and barian feldspars from picritic sill intruding to sediments in Rovina (Prague Basin, Czech Republic). We discuss the temperatures of their formation and suggest the likely genesis. Observations and evaluation of this curious slawsonite–celsian–hyalophane assemblage provide valuable information on feldspars phase equilibria, particularly in cases when one coexisting phase – slawsonite – has been noticed only rarely in nature.

FIELD RELATIONS AND PETROLOGY OF THE HOST PICRITE

The studied picrite sill, together with the underlying doleritic basalt intrusion, was emplaced within Ordovician (Hirnantian) quartzitic siltstones of the Kosov Fm. (N49° 55.412', E14° 13.320'). The bottom section of the outcrop is partially covered by Quaternary sediments, but the lower contact of the Kosov Fm. with Silurian (Llandovery) black calcareous shales of the Motol Fm. is clearly tectonic. It is represented by the so-called Koda Fault – a synsedimentary structure that was reactivated during Variscan orogeny to thrust Ordovician over the Silurian strata (Kříž 1991). The present-day picrite

92 outcrop is preserved in the form of several 1 m thick blocks exposed within ca. 15 m
93 wide zone on a vegetated slope.

94 The picrite shows a porphyric texture with idiomorphic olivine and clinopyroxene
95 phenocrysts. Modal composition determined on the basis of point counting by Fiala
96 (1947), and supplemented by our mineral analyses, is as follows: rare fresh olivine
97 phenocrysts (15.2 vol% – $Fo_{74–78}$) are intensely replaced by serpentine (28.7 vol%) with
98 chlorite (25.6 vol% – Mg-rich chlorite) and usually bear spinel inclusions. Clinopyroxene
99 phenocrysts (6.8 vol% – diopside, hedenbergite) carry tiny spinel (ulvöspinel, magnetite)
100 and ilmenite inclusions; the phenocrysts form poikilitic intergrowths with plagioclase (9.8
101 vol% – $An_{70–84}$) and olivine. Ilmenite and spinel account for 1.9 vol% of the rock.
102 Biotites (0.7 vol%) overgrow ilmenite and form transition zones to the interstitial matrix
103 (11.3 vol%), which is dominated by chlorite. Partially decomposed plagioclases, chlorite
104 pseudomorphs after calcic amphibole, apatite, ilmenite and spinel constitute the matrix.
105 Recently, secondary mineral assemblage consisting of slawsonite, celsian, hyalophane,
106 vuagnatite, hydrogrossular and pectolite has been identified in the interstitial phase by
107 back-scattered electron (BSE) imaging.

108 ## ANALYTICAL METHODS

109 Representative picrite (20 kg) and basalt (40 kg) samples were collected in the
110 field, crushed, homogenized and ground in an agate mill. Major-element analyses were
111 carried out at the Central Laboratories of the Czech Geological Survey, Prague (wet
112 silicate analyses: FAAS, ICP-OES, PMT, IR spectrometry). The trace-element data came
113 from Activation Laboratories, Vancouver (ICP-MS package 4B2 Research, sample
114 dissolution by a lithium metaborate/tetraborate fusion followed by rapid digestion in a

115 weak nitric acid solution). Whole-rock data were processed by the GCDkit package
116 (Janoušek et al. 2006). Analyses and compositional maps of the picrite mineral
117 assemblage were obtained using the scanning electron microscope TESCAN Vega
118 equipped with EDS detector X-Max 50 (Oxford Instruments) at the Institute of Petrology
119 and Structural Geology (Faculty of Science, Charles University in Prague). The raw data
120 were processed with INCA software, employing the XPP matrix correction procedure
121 (Pouchou and Pichoir 1988). Standards used with X-ray lines in parentheses were albite
122 (Na *Kα*), sanidine (K, Si *Kα*), synthetic garnet (Al *Kα*), wollastonite (Ca *Kα*), celestine
123 (Sr *Lα*), barite (Ba *Lα*), olivine (Mg *Kα*), almandine (Fe *Kα*), rhodonite (Mn *Kα*),
124 pentlandite (Ni *Kα*), rutile (Ti *Kα*), Cr_2O_3 (Cr *Kα*) and vanadium (V *Kα*); the detection
125 limits were typically 0.1 wt% of the respective element. All analyses were obtained at 15
126 kV acceleration voltage and 1.5 nA beam current with a rastered 3×3 μm beam. Time
127 tests showed no elemental mobilization under these conditions. The compositional
128 variations of samples are represented by maps of X-ray intensity at defined energy
129 intervals. The effect of interference of Sr and Si peaks was suppressed by manual
130 adjustment of the considered energy range. However, only the picrite feldspars were
131 suitable for EDS analyses, because the barian feldspars in the basalt intrusion were
132 smaller than the beam current resolution.

133 In total, twelve analyses of a single slawsonite grain, representative analyses of
134 one hundred and twenty-seven celsian and of nine hyalophane grains, and two analyses of
135 discontinuously zoned barian feldspar obtained from seven thin sections of the picrite are
136 the subject of this paper. Representative analyses of hydrogrossular, vuagnatite, pectolite,
137 plagioclase, olivine, clinopyroxene, spinel, amphibole, chlorite, serpentine, talc and

ilmenite are provided in the Appendix. In case of hydrogrossular, OH = (3–Si)×4 substituting silica was determined from stoichiometry for 8(cations + OH/4). Results of chlorite thermometry calculations (Kranidiotis and MacLean 1987) are also listed in the Appendix.

RESULTS

Whole-rock geochemistry of the host basic volcanics

On the basis of the total alkalis vs. silica diagram (TAS; Le Bas et al. 1986), Rovina picrite is characterized as a subalkaline picrobasalt and the underlying doleritic intrusion is a basalt, falling at the boundary between the alkaline and subalkaline domains (Fig. 1a).

Compared to NMORB (Fig. 1b; Sun and McDonough 1989), the basalt is rich in incompatible elements (Zr_N = 2.0), while the picrite is depleted (Zr_N = 0.7). The positive anomaly of Ba, the most prominent feature of both samples, corresponds to concentrations of 2,460 ppm (Ba_N = 390.5) in the picrite and of 550 ppm (Ba_N =87.3) in the basalt. Also Sr concentrations are elevated (167 ppm in the picrite and 428 ppm in the basalt). Moreover, the NMORB-normalized patterns show positive anomalies of Ti, elevated Cs in the picrite (Cs in the basalt was below detection limit of 0.1 ppm) and a distinct trough for K in the basalt.

The chondrite-normalized (Boynton 1984) REE patterns (Fig. 1c) are characterized by a moderate LREE over HREE enrichment (La_N/Yb_N = 3.5–4.0) and near linear courses lacking any Eu anomaly (Eu/Eu^* = 1.0).

Chemical composition and textures of strontian and barian feldspars

The BSE images reveal common barian feldspars and rare slawsonite in the interstitial phase between olivine and diopside phenocrysts and rare barian feldspars enclosed within diopsides (Fig. 2). Mode of occurrence of the barian feldspars is characterized in most cases by thin and rough mantling of plagioclase grains (Fig. 2a). These celsian-rim zones separate the plagioclases from hydrogrossular ($Ca_3Al_2(SiO4)_{3-x}(OH)_{4x}$; Hgr) and vuagnatite ($CaAlSiO_4(OH)$; Vgt). Rarer are small plagioclase laths enclosed within the diopside phenocrysts, which are completely replaced by celsian, talc and possibly by Ca–Al silicate (Hgr or Vgt?) closely intergrown with Mg-rich mineral (serpentine or chlorite?; Fig. 2b). With the exception of talc, only mixture analyses were obtained from the original plagioclase due to small size of grains and their intergrowth. Described textures suggest resorption of original plagioclases followed by precipitation of Ba-rich feldspars, vuagnatite and hydrogrossular.

Only one slawsonite grain has been detected in the seven thin sections of the Rovina picrite sample (Fig. 2a, c). The slawsonite replaces an original bytownite (An_{77}) lath (Fig. 2c), exhibits undulatory extinction, and is approximately 50 μm across. The slawsonite composition varies from $Sl_{91}Cn_3An_3Ab_3$ (core) to $Sl_{82}Cn_3An_4Ab_9Or_2$ (rim). The BSE image (Fig. 2c) indicates the negligible content of Ba-rich inclusions. The slawsonite is rimmed by vuagnatite and celsian, which apparently infill fissures cutting the slawsonite grain. Chlorite and a serpentine–chlorite mixture were detected at the upper rim of the slawsonite grain.

The analyzed barian feldspars contain 27–41 wt% BaO, and the strontian feldspars 26–28 wt% SrO (Tab. 1). The nomenclature of the barian feldspars follows

Essene et al. (2005): celsian > 75 mol% Cn, hyalophane > 15 mol% and < 75 mol% Cn. An analysis of discontinuously zoned barian feldspar (Fig. 2d) revealed a hyalophane core $Cn_{64.4}An_{1.1}Ab_{2.4}Or_{31.6}Sl_{0.5}$ and a celsian rim $Cn_{91.8}An_{2.3}Ab_{0.5}Or_{4.7}Sl_{0.7}$. The composition of interstitial celsians varies from $Cn_{96.9}An_{0.3}Ab_{0.2}Or_{2}Sl_{0.6}$ to $Cn_{76.3}An_{4.7}Ab_{3}Or_{15.7}Sl_{0.3,}$ and the hyalophanes range from $Cn_{72.2}An_{1.4}Ab_{5.1}Or_{21.1}Sl_{0.2}$ to $Cn_{57.3}An_{0.8}Ab_{3.1}Or_{38.5}Sl_{0.3}$ (Fig. 3).

Celsians and hyalophanes form rather thin rims, which cannot be readily distinguished from plagioclase under the optical microscope (Fig. 4a, b). Barium and strontium distribution maps (Fig. 4c, d) suggest the normal zoning of SrO and the reverse zoning of BaO in barian feldspars overgrowing the original plagioclases of $An_{70–84}$. The calcium distribution map (Fig. 3e) clearly distinguishes two other components enclosing plagioclases – vuagnatite from hydrogrossular. In addition, pectolite [$NaCa_2Si_3O_8(OH)$; Pct] was identified in the vuagnatite by the use of sodium distribution map (Fig. 3f).

DISCUSSION

Comparison with published data

Among the reported natural slawsonites, the composition of the studied grain (82–91 mol% of Sl and 3–4 mol% of Cn) bears a striking resemblance to that from the Sarusaka ultramafic xenolith described by Matsubara (1985). This author assumed a low-*T* origin of the slawsonite–celsian assemblage (*ca.* 300–400 °C) and ruled out any significant substitution of Sr in celsian. The latter is also true for the Rovina celsians, in which the SrO content in barian feldspars does not exceed 0.75 wt% (2.6 mol% Sl).

Celsians (97–76 mol% of Cn) and hyalophanes (72–57 mol% of Cn) replace bytownites ($An_{70–84}$) in the studied picrite. Element distribution maps document that the

celsians and hyalophanes attain maximal SrO concentrations next to the bytownites (Fig. 4d) and that BaO concentrations increase rimwards (i.e., as the barian feldspar grew; Fig. 2d, 4c). This could be caused by the incompatibility of Ba in the denser structure of the calcic plagioclase (Blundy and Wood 1991) during bytownite dissolution.

The entire dataset acquired spans the miscibility field of the ternary (Ba, K, Na)-feldspar system (Lagache and Catel 1992; Viswanathan 1992). Single discontinuously zoned feldspar (Fig. 2d), sufficiently large to obtain EDS analyses, with a hyalophane core (64 mol% Cn) rimmed by celsian (91 mol% Cn), could indicate the possibility of a solvus gap between celsian and hyalophane (Essene et al. 2005).

Albite content in barian feldspars correlates positively with T (Pan and Fleet 1991; Chabu and Boulègue 1992; Morishita 2005). Essene et al. (2005) proposed a geothermometer on the basis of observations of barian feldspars with various Ab contents in rocks metamorphosed by various grades. The Ab contents of celsians and hyalophanes in the picrite vary from 0.1 to 6.7 mol%, which is, according to Essene et al. (2005), characteristic of diagenetic conditions (T = 100–250 °C). Nevertheless, the amount of Na in barian feldspar increases when buffered by albite. Hence, given the absence of albite in the Rovina picrite, the geothermometer is not applicable to our dataset.

Constrains on slawsonite–celsian–hyalophane genesis

Taking into account the partial dissolution of bytownites, replacement textures and the reverse zoning of BaO in Ba-feldspars, we suggest that the studied slawsonite, celsians and hyalophanes were not in equilibrium with the picrite magma. An introduction of the necessary Sr and Ba due to crustal contamination of the intruding magma is highly improbable, as the Sr- and Ba-rich phases replace the already

crystallized idiomorphic plagioclases. Most importantly, the picrite shows a pristine basaltic whole-rock geochemical signature with superimposed sharp Ba and Sr spikes (Fig. 1). In addition, apparent loss of K in the basalt is a characteristic feature of low *T* (70–150 °C) basalt–seawater alteration (Bloch and Bischoff 1979; Seyfried 1979) and elevated concentration of Cs (0.9 ppm) in picrite relate to very low *T* stages of alteration and weathering (Hart et al. 1974). All these observations point to syn- or even post-depositional subsolidus open-system processes, most probably due to an interaction with fluids, rather than to an equilibration of crustal material with basaltic magma.

Textural relationships and the presence of vuagnatite, hydrogrossular and pectolite provide a valuable insight into genesis of the Sr- and Ba-rich phases. Vuagnatite, hydrogrossular and pectolite had been considered as products of rodingitization derived from replacement of plagioclase under the conditions of prehnite–pumpellyite facies (Sarp et al. 1976; Matsubara et al. 1977; Barriga and Fyfe 1983; Palandri and Reed 2004; Li et al. 2007; Bach et al. 2013). Rodingitization is a type of Ca-metasomatism leading to depletion of SiO_2 and Na_2O, which ideally occurs at $T < 350$ °C (Pirajno 2013). Rodingitization and serpentinization take place contemporaneously. The former is not caused by Ca-rich nature of serpentinization fluids but by the stability of Ca-silicates (i.e. hydrogrossular; Bach and Klein, 2009). Hence, the principal metasomatic mechanism of rodingitization is not a calcium addition but more importantly a silica loss during serpentinization process (Frost and Beard 2007; Frost et al. 2008; Bach et al. 2013).

Taking into account constrains on genesis of the other reported Sr- and Ba-silicates, stronalsite and banalsite (Hori et al. 1987), which formed under silica-poor

conditions, we could infer that silica loss connected to rodingitization and serpentinization could represent a viable mechanism for formation of strontian and barian feldspars in our case. Moreover, Hori et al. (1987) suggested that at slightly Si-richer conditions, during decomposition of plagioclase to any Sr-excluding mineral such as hydrogrossular, formation of slawsonite instead of stronalsite would be favored. Besides that, Liferovich et al. (2006) proposed three major mechanisms for genesis of stronalsite and banalsite: crystallization from a silica-undersaturated sodic magma, formation during high-grade metamorphism and, the most common, deuteric alteration of feldspathoid-bearing igneous rocks. None could reflect likely genesis of slawsonite, celsians and hyalophanes from the Rovina picrite – Ba and Sr concentrations are too high for primary magmatic composition, the picrite and any rocks within the Prague Basin are essentially unmetamorphosed (Chlupáč et al. 1998), and deuteric alteration would require contamination by crustal rocks, which would not preserve the rest of primary magmatic signature of the picrite (Fig. 1).

A possible clue to strontian and barian feldspar genesis in the studied picrite could be based on thermodynamic modeling of micro-rodingitization of olivine-rich troctolites (Frost et al. 2008). Thermodynamic reactions of plagioclase alteration to prehnite and grossular/hydrogrossular accompanied by serpentinization and chloritization of olivine were calculated by Frost et al. (2008) for maximum $T = 350$ °C (based on a lower stability limit of clinozoisite) and $P = 0.1$ GPa. Since vuagnatite shows the same mode of occurrence as prehnite, the former merely requiring more silica-deficient conditions (Matsubara et al. 1977), the micro-rodingitization model could be adopted for the Rovina picrite.

Hence, desilication of plagioclase to vuagnatite/hydrogrossular and serpentinization of olivine could have taken place simultaneously in the Rovina picrite. If true, the alteration reactions would have involved surplus H_2O, SrO and BaO (Fig. 5). We suggest an addition of SrO and BaO by a fluid as celsians even replace plagioclase inclusions in magmatic diopside. The possibility that Ba and Sr were in situ products of original plagioclase decomposition requires a late-magmatic contamination of the picrite. Such case could be expressed by an accommodation of Ba and Sr in outer zones of interstitial plagioclases that were subsequently dissolved. On the contrary, Ba and Sr would not have been accommodated in plagioclases, which were fully crystallized before the diopside growth had been completed. At first, decomposition of plagioclase to vuagnatite occurred, releasing silica and alumina for the reaction of slawsonite or celsian with BaO and SrO supplied by the fluid:

1. $2CaAl_2Si_2O_8 + H_2O \rightarrow 2CaAlSiO_4(OH) + Al_2O_{3(aq.)} + 2SiO_{2(aq.)}$
   anorthite *vuagnatite*

2a. $SrO_{(aq.)} + Al_2O_{3(aq.)} + 2SiO_{2(aq.)} \rightarrow SrAl_2Si_2O_8$
slawsonite

or

2b. $BaO_{(aq.)} + Al_2O_{3(aq.)} + 2SiO_{2(aq.)} \rightarrow BaAl_2Si_2O_8$
celsian

Genesis of slawsonite and celsian was most likely triggered by decomposition of plagioclase and these minerals precipitated directly from the fluid. Slawsonite seems the older phase because it is cut by veintlets filled by celsian. As the plagioclase is not a pure

anorthite but bytownite, the excess of Na could have been either compensated by a formation of pectolite or lost from the system. Furthermore, vuagnatite was transformed to hydrogrossular:

3. $6CaAlSiO_4(OH) + H_2O \rightarrow 2Ca_3Al_2(SiO_4)_2(OH)_4 + Al_2O_{3(aq.)} + 2SiO_{2(aq.)}$
   vuagnatite *hydrogrossular*

Hydrogrossular could also originate by the reaction: $3CaAl_2Si_2O_8 + 2H_2O \rightarrow Ca_3Al_2(SiO_4)_2(OH)_4 + Al_2O_{3(aq.)} + 4SiO_{2(aq.)}$. However, hydrogrossulars enclosed wihin vuagnatites (Fig. 3e) indicate that vuagnatite decomposition was their most probable genesis. Excess silica provided by plagioclase dissolution was consumed by contemporaneous serpentinization of olivine:

4. $3Mg_2SiO_4 + SiO_{2(aq.)} \rightarrow 2Mg_3Si_2O_5(OH)_4$
   forsterite *serpentine*

Alumina released by desilication led to the formation of chlorite and rarely talc from serpentine and closed the rodingitization of the Rovina picrite:

5. $Mg_3Si_2O_5(OH)_4 + Al_2O_{3(aq.)} + H_2O \rightarrow Mg_5Al_2Si_3O_{10}(OH)_8 + SiO_{2(aq.)}$
   serpentine *chlorite*

In summary, strontian and barian feldspars genesis was most probably connected to diffusional metasomatism – rodingitization and serpentinization reactions, which were caused by $SrO–BaO–H_2O$ intergranular fluid infiltration. Such reactions could operate at

$T \leq 350$ °C, which represents lower stability limit of clinozoisite. The lower limit of T range suitable for proposed reactions could be constrained by the use of a chlorite thermometer, as chlorites represent the final stage of the Rovina picrite alteration. Discussion on chlorite thermometry (de Caritat et al. 1993) provides variable approaches on T calculations. For chlorites in Al-saturated environment, e.g., in the presence of other aluminous minerals, the Kranidiotis and MacLean (1987) thermometer is the most convenient one. Its calculation (Appendix) gives T range ca. 320–160 °C. Pressure constraint provides a transition of celsian to cymrite, which occurs at $P \sim 0.5$ GPa and 350 °C (Graham et al. 1992).

The source of Ba and Sr, enriched in the picrite and basalt, is a matter for discussion. Morishita (2005) suggested that Ba and Sr are important constituents in fluids related to the formation of metasomatized rocks in serpentinite–matrix mélanges formed during subduction, which dehydrated Ba-rich sediments – a possible source for Ba-bearing fluids. The Prague Basin, on the contrary, represented a different tectonic setting – rifted basin – during Ordovician (Havlíček 1982). Moreover, the process of rodingitization is characteristic of seafloor metasomatism associated with serpentinization (Pirajno 2013). Thus, range of formation T (350–160 °C) of the Ba- and Sr- feldspars points to their post-magmatic origin due to seafloor metasomatism.

CONCLUDING REMARKS AND IMPLICATIONS

The whole-rock geochemical signature of the Late Ordovician picrite sill and the underlying doleritic basalt intrusion are characterized by eye-catching enrichment in Ba and Sr. The accommodation of such significant amounts of Ba and Sr in rock samples resulted in the precipitation of a common barian (celsian and hyalophane) and a rare

strontian (slawsonite) feldspar assemblage, filling the interstitial space between the olivine and diopside phenocrysts. This represents the first known occurrence of slawsonite in Europe. From the study of this feldspar assemblage in the picrite, the following implications emerged:

1) Ba- and Sr-feldspars formed due to desilication of original plagioclases during interaction with SrO–BaO–H_2O fluid.

2) The surplus Sr and Ba was probably introduced by intergranular fluid during diffusional seafloor metasomatism (i.e. rodingitization and serpentinization).

2) Ba- and Sr-feldspars precipitated directly from fluid phase at 350 –160 °C and less than 0.5 GPa.

ACKNOWLEDGEMENTS

The authors are grateful to Milan Fišera and Stanislav Vrána for optical microscopy consultations and to Radmila Nahodilová for valuable comments on stability relations. This study was funded by the GA ČR (Czech Science Foundation) project 210/10/2351 and our special thanks are extended to the Strategic Research Plan of the Czech Geological Survey. We wish to acknowledge helpful reviews by Tomoaki Morishita, Axel Liebscher and Richard Yuretich, which markedly improved the quality of the paper.

REFERENCES CITED

Bach, W. and Klein, F. (2009) The petrology of seafloor rodingites: insights from geochemical reaction path modeling. Lithos, 112, 103–117.

Bach, W., Jöns, N. and Klein, F. (2013) Metasomatism within the ocean crust. In D.E. Harlov and H. Austrheim, Eds., Metasomatism and the Chemical Transformation of Rock: The Role of Fluids in Terrestrial and Extraterrestrial Processes, p. 253–288. Springer, Berlin.

Bambauer, H.U. and Nager, H.E. (1981) Gitterkonstanten und displazive Transformation synthetischer Erdalkalifeldspäte. I. System $CaAl_2Si_2O_8$–$SrAl_2Si_2O_8$–$BaAl_2Si_2O_8$. Neues Jahrbuch für Mineralogie Abhandlungen, 141, 225–239.

Barriga, F. and Fyfe, W.S. (1983) Development of rodingite in basaltic rocks in serpentinites, East Liguria, Italy. Contributions to Mineralogy and Petrology, 84, 146–151.

Bloch, S. and Bischoff, J.L. (1979) The effect of low-temperature alteration of basalt on the oceanic budget of potassium. Geology, 7, 193–196.

Blundy, J.D. and Wood, B.J. (1991) Crystal-chemical controls on the partitioning of Sr and Ba between plagioclase feldspar, silicate melts, and hydrothermal solutions. Geochimica et Cosmochimica Acta, 55, 193–209.

Boynton, W.V. (1984) Geochemistry of the rare elements: meteorite studies. In P. Henderson, Ed., Rare Earth Element Geochemistry, p. 63–114. Elsevier, Amsterdam.

Chabu, N. and Boulègue, J. (1992) Barian feldspar and muscovite from the Kipushi Zn–Pb–Cu deposit, Shaba, Zaire. The Canadian Mineralogist, 30, 1143–1152.

Chlupáč, I., Havlíček, V., Kříž, J., Kukal, Z. and Štorch, P. (1998) Palaeozoic of the Barrandian (Cambrian to Devonian), 183 p., Czech Geological Survey, Prague.

De Caritat, P., Hutcheon, I. and Walshe, J.L. (1993) Chlorite geothermometry: A review. Clays and Clay Minerals, 41, 219–239.

Deer, W.A., Howie, R.A., and Zussman, J. (1992) An Introduction to the Rock-Forming Minerals, 2nd ed., 696 p., Pearson Education Ltd., London.

———, ———, ——— (2001) Rock-forming minerals: feldspars, Vol. 4A, 2nd ed., 992 p., The Geological Society, London.

Essene, E.J., Claflin, C.L., Giorgetti, G., Mata, P.M., Peacor, D.R., Árkai, P., and Rathmell, M.A. (2005) Two-, three- and four-feldspar assemblages with hyalophane and celsian: implications for phase equilibria in $BaAl_2Si_2O_8$–$CaAl_2Si_2O_8$–$NaAlSi_3O_8$–$KAlSi_3O_8$. European Journal of Mineralogy, 17, 515–535.

Fiala, F. (1947) Diabasové pikrity v Barrandienu (Mořinka, Rovina, Sedlec). Věstník Královské české společnosti nauk, 19, 1–55.

Frost, B.R. and Beard, J.S. (2007) On silica activity and serpentinization. Journal of Petrology, 48, 1351–1368.

———, ———, McCaig, A. and Condliffe, E. (2008) The formation of micro-rodingites from IODP Hole U1309D: key to understanding the process of serpentinization. Journal of Petrology, 49, 1579–1588.

Gay, P. and Roy, N.N. (1968) The mineralogy of the potassium–barium feldspar series: III. Subsolidus relationships. Mineralogical Magazine, 36, 914–932.

Graham, C.M., Tareen, J.A.K., McMillan, P.F. and Lowe, B.M. (1992) An experimental and thermodynamic study of cymrite and celsian stability in the system BaO–Al_2O_3–SiO_2–H_2O. European Journal of Mineralogy, 4, 251–269.

Griffen, D.T. and Ribbe, P.H. (1976) Refinement of the crystal structure of celsian. American Mineralogist, 61, 414–418.

———, ———, and Gibbs, G.V. (1977) The structure of slawsonite, a strontium analogue of paracelsian. American Mineralogist, 62, 31–35.

Hart, S.R., Erlank, A.J. and Kable, E.J.D. (1974) Sea floor basalt alteration: Some chemical and Sr isotopic effects. Contributions to Mineralogy and Petrology, 44, 219–230.

Havlíček, V. (1982) Ordovician in the Bohemia: Development of the Prague Basin and its benthic communities. Sborník Geologických Věd, 37, 103–136.

Hori, H., Nakai, I., Nagashima, K., Matsubara, S. and Kato, A. (1987) Stronalsite, $SrNa_2Al_4Si_4O_{16}$, a new mineral from Rendai, Kochi City, Japan. Mineralogical Journal, 13, 368–375.

Irvine, T.N. and Baragar, W.R.A. (1971) A guide to the chemical classification of the common volcanic rocks. Canadian Journal of Earth Sciences, 8**,** 523–548.

Janoušek, V., Farrow, C.M., and Erban, V. (2006) Interpretation of whole-rock geochemical data in igneous geochemistry: introducing Geochemical Data Toolkit (GCDkit). Journal of Petrology, 47, 1255–1259.

Kranidiotis, P. and MacLean (1987) Systematics of chlorite alteration at the Phelps Dodge massive sulfide deposits, Matagama, Quebec. Economic Geology, 82, 1898–1911.

Kříž, J. (1991) The Silurian of the Prague Basin (Bohemia) – tectonic eustatic and volcanic controls on facies and faunal development. In M.G. Bassett, P.D. Lane and D. Edwards, Eds., The Murchison Symposium: Proceedings of an

International Conference on The Silurian System. Special Papers in Palaeontology, 44, 179–203.

Lagache, M. and Catel, N. (1992) Solid solution and unmixing in the (Ba,K,Na)-feldspars. Part I. The albite–celsian solvus determined by ion-exchange experiments. European Journal of Mineralogy, 4, 209–212.

Le Bas, M.J., Le Maitre, R.W., Streckeisen, A., and Zanettin, B. (1986) A chemical classification of volcanic rocks based on the total alkali–silica diagram. Journal of Petrology, 27, 745–750.

Li, X.P., Zhang, L., Wei, C., Al, Y. and Chen, J. (2007) Petrology of rodingite derived from eclogite in western Tianshan, China. Journal of Metamorphic Geology, 25, 363–382.

Liferovich, R.P., Mitchell, R.H., Zozulya, D.R. and Shpachenko, A.K. (2006) Paragenesis and composition of banalsite, stronalsite, and their solid solution in nepheline syenite and ultramafic alkaline rocks. Canadian Mineralogist, 44, 929–942.

Lin, H.C. and Foster, W.R. (1968) Studies in the system $BaO–Al_2O_3–SiO_2$. I. The polymorphism of celsian. American Mineralogist, 53, 134–144.

Matsubara, S. (1985) The mineralogical implication of barium and strontium silicates. Bulletin of the National Science Museum Series C, 11, 37–96.

———, Kato, A. and Sakurai, K. (1997) The occurrence of vuagnatite from Shiraki, Toba, Mie Prefecture, Japan. Bulletin of the National Science Museum Series C, 3, 41–48.

McCauley, R.A. (2000) Polymorphism and dielectric electric properties of Ba- and Sr-containing feldspars. Journal of Materials Science, 35, 3939–3942.

Morishita, T. (2005) Occurrence and chemical composition of barian feldspars in a jadeitite from the Itoigawa-Ohmi district in the Renge high-P/T-type metamorphic belt, Japan. Mineralogical Magazine, 69, 39–51.

Nakajima, T., Maruyama, S. and Matsuoka K. (1978) Metamorphism of the green rocks of the Ino Formation in central Shikoku. Journal of the Japanese Association of Mineralogists, Petrologists and Economic Geologists, 84, 729–737.

Palandri, J.L. and Reed, M.H. (2004) Geochemical models of metasomatism in ultramafic systems: serpentinization, rodingitization and sea floor carbonate chimney precipitation. Geochimica et Cosmochimica Acta, 68, 1115–1133.

Pan, Y. and Fleet, M.E. (1991) Barian feldspar and barian–chromian muscovite from the Hemlo area, Ontario. The Canadian Mineralogist, 29, 481–498.

Pirajno, F. (2013) Effects of metasomatism on mineral systems and their host rocks: alkali metasomatism, skarns, greisens, tourmalinites, rodingites, black-wall alteration and listvenites. In D.E. Harlov and H. Austrheim, Eds., Metasomatism and the Chemical Transformation of Rock: The Role of Fluids in Terrestrial and Extraterrestrial Processes, p. 203–251. Springer, Berlin.

Pouchou, J.L. and Pichoir, F. (1988) Determination of mass absorption coefficients for soft X-rays by use of the electron microprobe. In D.E. Newbury, Ed., Microbeam analysis, p. 319–324. San Francisco Press, San Francisco.

Sarp, H., Bertrand, J. and McNear, E. (1976) Vuagnatite, $CaAl(OH)SiO_4$, a new natural calcium aluminium nesosilicate. American Mineralogist, 61, 825–830.

Seyfried, W.E. Jr. (1979) Low temperature basalt alteration by sea water: an experimental study at 70°C and 150°C. Geochimica et Cosmochimica Acta, 43, 1937–1947.

Sun, S. and McDonough, W.F. (1989) Chemical and isotope systematics of oceanic basalts: implications for mantle composition and processes. In A.D. Saunders and M.J. Norry, Eds., Magmatism in the Ocean Basins, Special Publications 42, p. 313–345. The Geological Society, London.

Tagai, T., Hoschi, T., and Suzuki, M. (1995) A new modification of slawsonite, $SrAl_2Si_2O_8$: its structure and phase transition. Zeitschrift für Kristallographie, 210, 741–745.

Viswanathan, K. (1992) Solid solution and unmixing in the (Ba,K,Na)-feldspars. Part II: an X-ray powder diffraction study of the ternary feldspars. European Journal of Mineralogy, 4, 213–216.

——— and Harneit, O. (1989) Solid-solution and unmixing in the feldspar system, albite ($NaAlSi_3O_8$)–celsian ($BaAl_2Si_2O_8$). European Journal of Mineralogy, 1, 239–248.

FIGURE CAPTIONS

Figure 1. Whole-rock geochemical analyses of the Rovina picrite and basalt. (a) TAS diagram (Le Bas et al. 1986; dividing line between the subalkaline and alkaline domains after Irvine and Baragar 1971). (b) Spiderplot normalized by average NMORB composition with model courses of the OIB and EMORB reservoirs (from Sun and McDonough 1989). (c) Chondrite-normalized (Boynton 1984) REE patterns.

Figure 2. Back-scattered electron images with positions of EDS analyses. (a) Interstitial phase – slawsonite and celsians. Rectangle indicates position of Fig. 4. (b) Original

plagioclase enclosed within diopside. Ca+Al+Si+Mg stand for mixture analysis of Ca–Al silicate (hydrogrossular or vuagnatite) and Mg mineral (serpentine or chlorite). (c) Slawsonite. (Dark stain below position of Sl_4 analysis represents surface external inpurity.) (d) Discontinuously zoned barian feldspar. An = anorthite; Chl = chlorite; Cn = celsian, Di = diopside; Fo = forsterite; Hgr = hydrogrossular; Hy = hyalophane; Sl = slawsonite; Sp = spinel; Srp = serpentine; Tlc = talc; Vgt = vuagnatite. Chlorite *T* after Kranidiotis and MacLean (1987).

Figure 3. Analyses of barian and strontian feldspars with An content < 6 mol% in the ternary plots $NaAl_2Si_2O_8$–$KAlSi_3O_8$–($SrAl_2Si_2O_8$ + $BaAl_2Si_2O_8$) (a) and $BaAl_2Si_2O_8$–$KAlSi_3O_8$–$SrAl_2Si_2O_8$ (b).

Figure 4. Microphotograph of interstitial mineral assemblage: Plane polarized light (a) and crossed polars (b) Element distribution maps of Ba (c), Sr (d), Ca (e), and Na (f). An = anorthite; Chl = chlorite; Cn = celsian; Hgr = hydrogrossular; Pct = pectolite; Sl = slawsonite; Vgt = vuagnatite.

Figure 5. Schematic sketch of textural relationships and reactions that operated during the alteration of plagioclase and olivine in the picrite.

TABLES

Table 1. Selected strontium and barium feldspar analyses (wt%) recalculated to structural formulae (apfu) and end members (mol%).

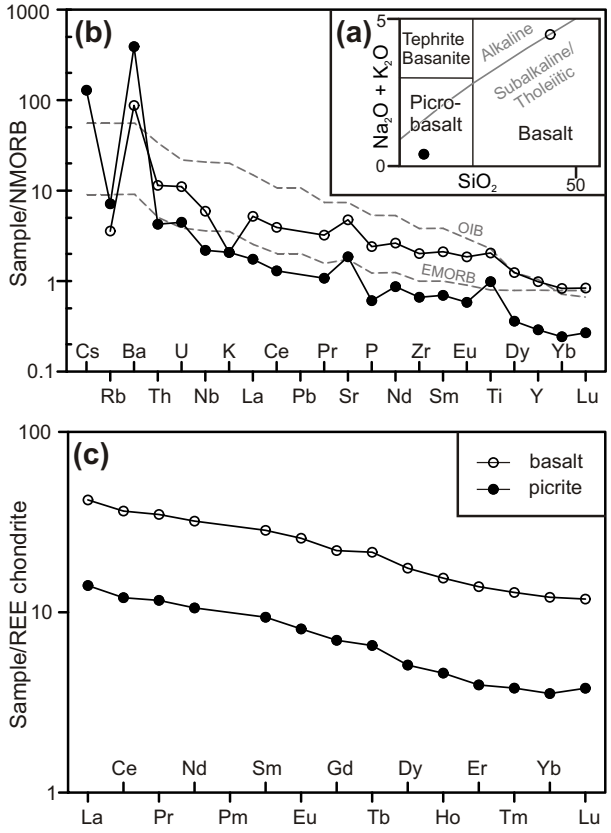
(a)
Tephrite
Basanite
Picro-
basalt
Basalt
Alkaline
Subalkaline/
Tholeiitic
Na2O + K2O
SiO2
5
0
50
(b)
Sample/NMORB
1000
100
10
1
0.1
OIB
EMORB
Cs Ba U K Ce Pr P Zr Eu Dy Yb
Rb Th Nb La Pb Sr Nd Sm Ti Y Lu
(c)
basalt
picrite
Sample/REE chondrite
100
10
1
Ce Nd Sm Gd Dy Er Yb
La Pr Pm Eu Tb Ho Tm Lu

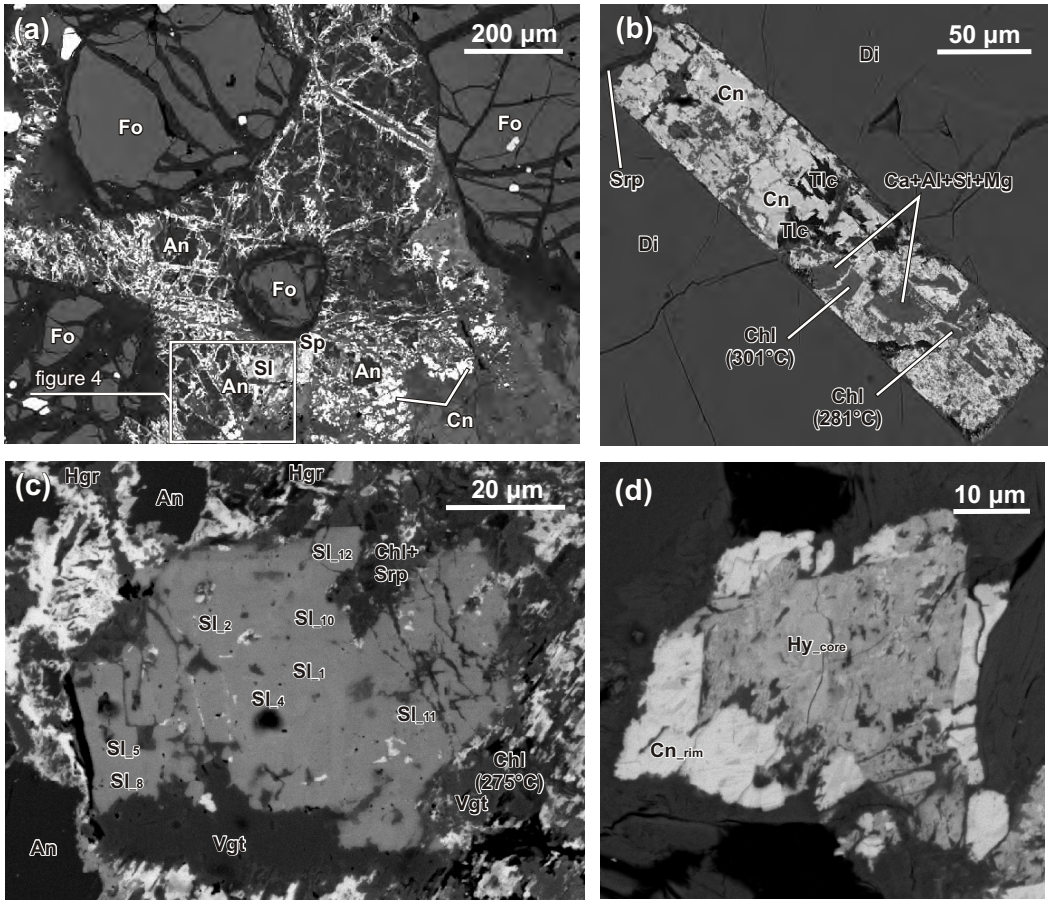
(a)
200 µm
Fo
Fo
An
Fo
Fo
Sp
Sl
An
An
figure 4
Cn
(b)
50 µm
Di
Cn
Srp
Tlc
Ca+Al+Si+Mg
Cn
Tlc
Di
Chl
(301°C)
Chl
(281°C)
(c)
Hgr
Hgr
An
20 µm
Sl_12
Chl+
Srp
Sl_2
Sl_10
Sl_1
Sl_4
Sl_11
Sl_5
Sl_8
Chl
(275°C)
Vgt
An
Vgt
(d)
10 µm
Hy_core
Cn_rim

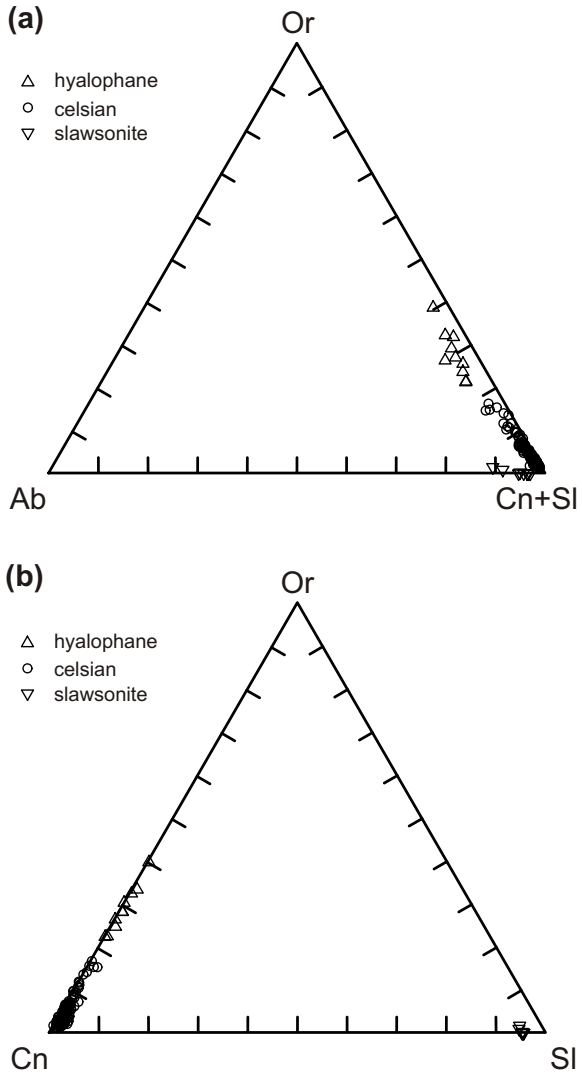
(a)
Or
hyalophane
celsian
slawsonite
Ab
Cn+Sl
(b)
Or
hyalophane
celsian
slawsonite
Cn
Sl

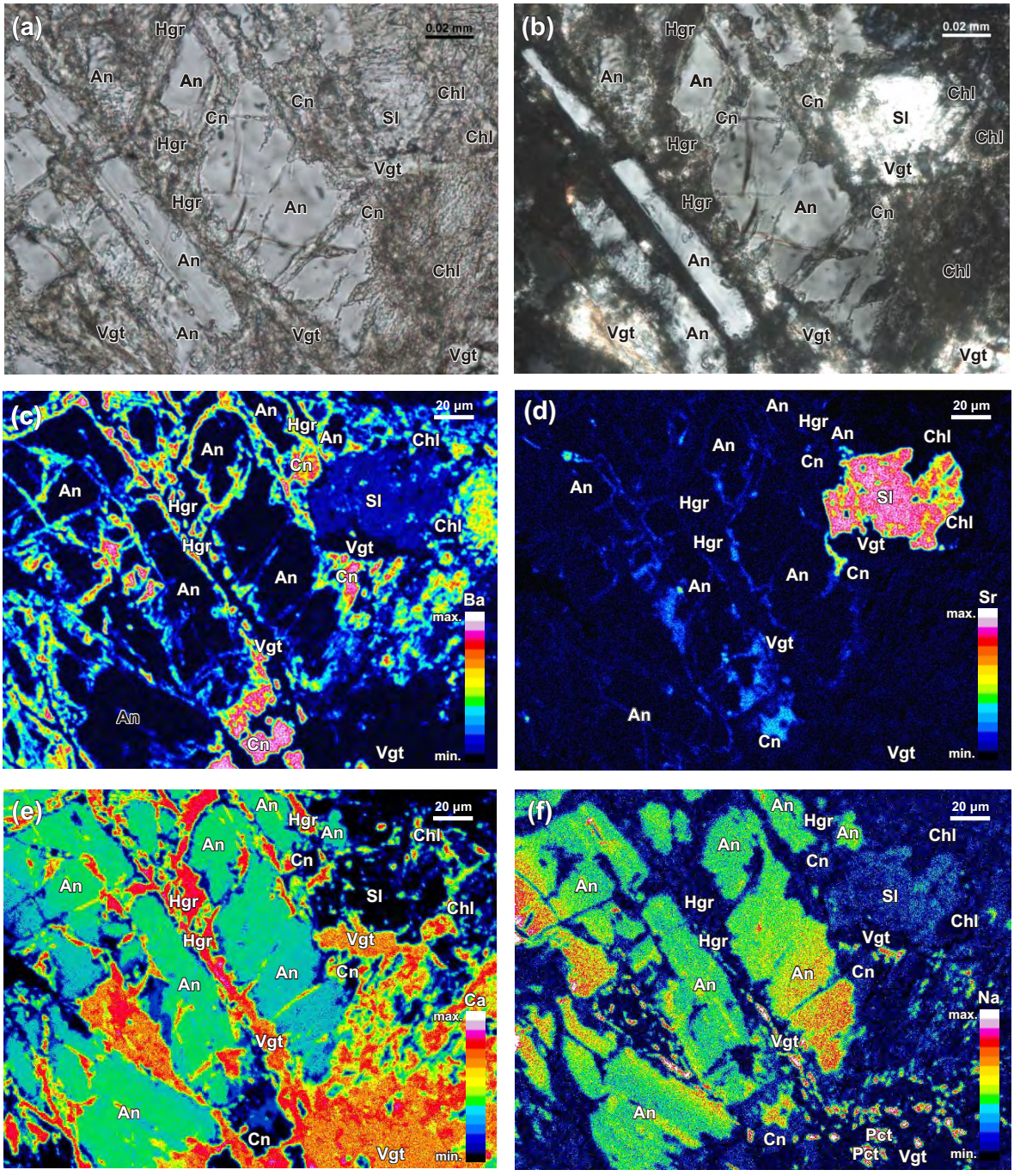
(a)
0.02 mm
Hgr
An
Cn
Chl
Sl
Vgt
(b)
0.02 mm
(c)
20 µm
Ba
max.
min.
(d)
20 µm
Sr
max.
min.
(e)
20 µm
Ca
max.
min.
(f)
20 µm
Na
max.
min.
Pct

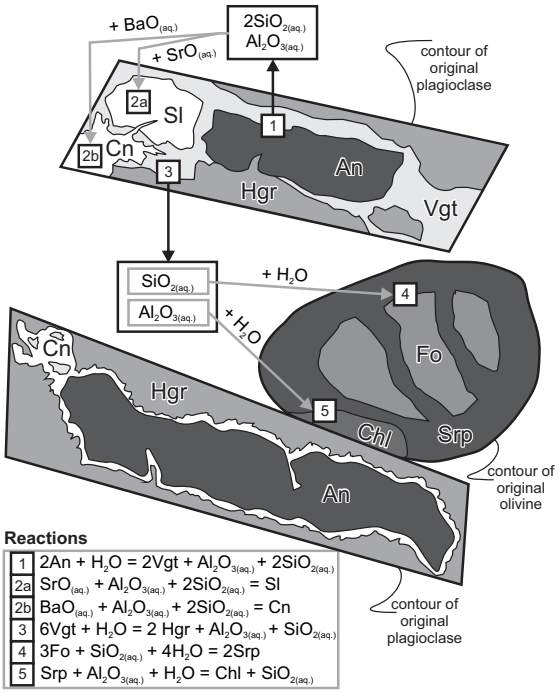

Reactions

1	$2An + H_2O = 2Vgt + Al_2O_{3(aq.)} + 2SiO_{2(aq.)}$
2a	$SrO_{(aq.)} + Al_2O_{3(aq.)} + 2SiO_{2(aq.)} = Sl$
2b	$BaO_{(aq.)} + Al_2O_{3(aq.)} + 2SiO_{2(aq.)} = Cn$
3	$6Vgt + H_2O = 2\ Hgr + Al_2O_{3(aq.)} + SiO_{2(aq.)}$
4	$3Fo + SiO_{2(aq.)} + 4H_2O = 2Srp$
5	$Srp + Al_2O_{3(aq.)} + H_2O = Chl + SiO_{2(aq.)}$

	SL_1	SL_2	SL_4	SL_5	SL_8	SL_10	SL_11	SL_12	Cn_1	Cn_2	Cn_117	Cn_128	Hy_1	Hy_10	Cn_rim	Hy_core
Na_2O	0.19	0.28	0.25	0.23	0.44	0.46	0.71	0.88	0.02	0.02	0.17	0.27	0.46	0.29	0.04	0.23
Al_2O_3	31.45	31.36	31.26	31.06	31.00	31.16	30.35	30.55	25.66	26.31	25.82	25.38	24.68	23.97	25.73	24.31
SiO_2	37.30	37.07	37.10	36.64	37.48	37.85	38.39	39.21	30.69	31.18	34.13	35.69	37.48	42.69	32.04	40.69
K_2O			0.02		0.06	0.03	0.14	0.24	0.26	0.37	1.48	2.18	2.92	5.58	0.62	4.52
CaO	0.54	0.55	0.51	0.67	0.62	0.82	0.71	0.60	0.05		0.13	0.78	0.22	0.13	0.37	0.19
FeO	0.15	0.14	0.13	0.07	0.19	0.20	0.17	0.36	0.16	0.27	0.43	0.29	0.29	0.10	0.58	0.41
SrO	28.24	28.29	27.86	28.04	27.78	26.98	26.26	26.03	0.17		0.17	0.10	0.06	0.11	0.22	0.15
BaO	1.55	1.23	1.69	1.75	1.67	1.68	1.75	1.53	41.32	39.97	37.11	34.62	32.43	27.06	39.93	29.99
Total (wt%)	99.42	98.93	98.83	98.46	99.21	99.18	98.48	99.39	98.33	98.12	99.43	99.32	98.55	99.94	99.54	100.47
Formulae (cations based on 8 oxygens)																
Na	0.02	0.03	0.03	0.02	0.05	0.05	0.07	0.09	0.00	0.00	0.02	0.03	0.05	0.03	0.01	0.03
Al	2.00	2.01	2.00	2.00	1.98	1.98	1.93	1.92	1.96	1.99	1.87	1.81	1.74	1.59	1.92	1.64
Si	2.02	2.01	2.02	2.01	2.03	2.04	2.08	2.09	1.99	2.00	2.10	2.15	2.24	2.40	2.03	2.33
K	0.00	0.00	0.00	0.00	0.00	0.00	0.01	0.02	0.02	0.03	0.12	0.17	0.22	0.40	0.05	0.33
Ca	0.03	0.03	0.03	0.04	0.04	0.05	0.04	0.03	0.00	0.00	0.01	0.05	0.01	0.01	0.02	0.01
Fe	0.00	0.00	0.00	0.00	0.00	0.01	0.00	0.01	0.01	0.01	0.01	0.01	0.01	0.00	0.02	0.01
Sr	0.88	0.89	0.88	0.89	0.87	0.84	0.82	0.81	0.01	0.00	0.01	0.00	0.00	0.00	0.01	0.00
Ba	0.03	0.03	0.04	0.04	0.04	0.04	0.04	0.03	1.05	1.00	0.89	0.82	0.76	0.60	0.99	0.67
Total (apfu)	4.99	5.00	5.00	5.00	5.01	5.00	5.00	5.00	5.04	5.03	5.03	5.04	5.03	5.03	5.04	5.03
End members																
An	3.23	3.25	3.05	3.97	3.61	4.87	4.18	3.53	0.30	0.00	0.83	4.68	1.35	0.78	2.29	1.10
Ab	2.07	3.01	2.74	2.48	4.62	4.92	7.60	9.28	0.21	0.22	1.90	2.97	5.12	3.06	0.50	2.40
Or	0.00	0.00	0.17	0.00	0.39	0.19	1.00	1.63	1.98	2.92	11.08	15.67	21.13	38.48	4.65	31.59
Cn	3.39	2.68	3.70	3.79	3.56	3.63	3.75	3.26	96.91	96.85	85.61	76.36	72.20	57.34	91.80	64.44
Sl	91.31	91.05	90.33	89.76	87.82	86.39	83.48	82.29	0.60	0.00	0.57	0.32	0.20	0.34	0.75	0.47